Structural characterization of the scale formed on a Ti–46Al–8Nb alloy oxidised in air at 700 °C

P.E. Tchoupé Ngnekou, M.-C. Lafont, F. Senocq, L. Laffont, B. Viguier, J. Lacaze*

CIRIMAT, Université de Toulouse, ENSIACET, 31077 Toulouse, France

A B S T R A C T

The structures of the oxide scale formed on a lamellar ($\gamma + \alpha_2$) Ti46Al8Nb alloy after heat-treatment in air at 700 °C for 50 and 1000 h have been compared. Though the outer scale is thicker after 1000 h, both oxide scales are similarly layered with an outer aluminium-rich layer. The main difference is that the aluminium-rich oxide is amorphous after 50 h while it becomes cubic gamma alumina after 1000 h. After 50 h, the presence of TiN was detected at the interface between the scale and the base metal. After 1000 h of oxidation, the subscale region is divided into two clearly separated zones differing by their composition, with a thick TiN layer close to the oxide scale. From these observations, it appears that the development of the oxide scale at 700 °C is similar to the scheme proposed in the literature for short times at higher temperatures, with the initial formation of a transient aluminium-rich oxide layer, which here is amorphous, and precipitates of TiN at the scale/metal interface that oxidise afterwards to rutile.

1. Introduction

Owing to their low density and their good mechanical properties, TiAl based intermetallics are considered to have a high potential for applications as structural materials at intermediate and high temperatures. Their oxidation resistance above 800 °C is however a concern because of the similar stability of Ti and Al in oxygen which can hinder the formation of a continuous protective alumina layer [1]. However, oxidation resistance may be improved by alloying [2], e.g. with niobium [3,4]. In their pioneer work, Choudhury et al. [3] noticed that TiAl is an alumina former when oxidised in oxygen and a titania former when oxidised in air, at 950 °C. These authors attributed this behaviour to the presence of nitrogen and excluded any effect of CO, CO_2 or water vapour. Later, Meier et al. [5] stressed the very peculiar oxidation behaviour of binary Al-rich TiAl alloys that form a continuous alumina layer in air at high temperature (1100–1350 °C) and in oxygen at much lower temperatures (800 °C), but not at high temperature. Apart for these particular conditions, it is most often reported that oxidation starts with the formation of alumina or of a mixture of alumina and TiO_2, but that further exposure leads to the development of an outer TiO_2 layer and an inner layer consisting in intermixed TiO_2 and Al_2O_3 grains in various proportions. A review of the literature leads to the conclusion that alloying with Nb delays the formation of the outer TiO_2 layer at any temperature whether in air or oxygen.

The so-called nitrogen effect associated to oxidation under air has been extensively studied and reviewed by Brady et al. [6]. According to Rakowski et al. [7], oxidation at 800–900 °C in air of a binary Ti–50Al (at.%) alloy leads to a scale of intermixed Al_2O_3 and TiN grains after 1 h. The TiN precipitates transform to TiO_2 with further oxidation while new TiN precipitates appear at the metal/scale interface. The scale gets layered with an outer TiO_2 layer and an inner layer made of TiO_2 and Al_2O_3. The same scale structure was found by Locci et al. [8] after long-term (6000 and 9000 h) oxidation of Ti–48Al–2Cr–2Nb at 704 °C in air. They also reported the presence of a continuous TiN layer at the metal/scale interface already formed after 1000 h of oxidation. In addition to the formation of TiN, other phases have been reported to appear at the interface between the scale and the oxide as well as in the subscale region as reviewed by Brady et al. [6] and Taniguchi and Shibata [2], amongst which are oxi-nitrides such as $Al_{27}O_{39}N$ [4], mixed nitride such as Ti_2AlN [4,9,10] and a cubic phase with a composition close to $Ti_5Al_3O_2$ [9,11,12] that has been called X or Z phase [6]. Other phases associated with Nb alloying are niobium oxide Nb_2O_5 [13], mixed oxides such as $AlNbO_4$ [14], $TiNb_2O_7$ [15], as well as $Ti_{36}Al_5Nb$ [4], Al_3Nb [16] and/or Al_2Nb [12]. Furthermore, recrystallization in the subscale has been repeatedly reported.

Because TiAl alloys are expected to operate at temperatures in the range 600–800 °C, we studied short term oxidation of such alloys at 700 °C under air at atmospheric pressure. Oxidation kinetics and preliminary observations by transmission electron

Corresponding author.
E-mail address: jacques.lacaze@ensiacet.fr (J. Lacaze).

microscopy have been reported previously for a TiAl–8Nb alloy [17]. It was found that the oxide scale consists of rutile TiO_2 and amorphous aluminium-rich oxide. Although X-rays indicated the presence of TiN, it could not be located in this previous study. The aim of the present work was thus to look at the oxide scale after further growth by studying samples oxidised for 1000 h, with particular emphasis on the detection of TiN.

2. Experimental details

The alloy under study was provided by the Interdisciplinary Research Centre (IRC) in Materials for High Performance Applications (Birmingham U.K.). Its composition was measured by GDMS (Shiva, Toulouse) in weight as 28.67% Al, 52.39% Ti, 18.70% Nb, with 160 ppm C, 53 ppm N, 2000 ppm O and 23 ppm H. For the major elements, the composition may be written as Ti–45.1Al–8.5Nb (in at.%). Small parallelepipedic samples ($10 \times 10 \times 1$ mm) were machined out of a cylindrical rod (20 mm in diameter and 70 mm in length). The samples were polished using SiC papers up to 4000 grade, then carefully washed in an ultrasonic bath containing acetone. Two types of isothermal oxidation experiments were carried out:

1 Thermogravimetric records in an SETARAM TAG-24 thermobalance for 50 h oxidizing treatment. A full account of the oxidation kinetics and characterization of the oxide scale with X-rays and transmission electron microscopy (TEM) has been given elsewhere [17]. The total mass gain was found to be 1.5 mg cm^{-2}.
2 1000 h treatment in an SiC furnace equipped with a muffle for atmosphere control.

In both cases, the atmosphere around the sample was first flushed with argon and then filled with synthetic air (20% O_2 and 80% N_2). The gas flow rate was afterwards kept constant at 0.4 L h^{-1} during the whole test for continuous renewal of the oxidizing environment. The samples were brought to 700 °C by a continuous heating at 1 °C s^{-1} and maintained at this temperature for either 50 h or 1000 h. Finally, the samples were allowed to cool to room temperature at a rate of 1 °C s^{-1} and removed from the furnace for analysis.

The surface of the samples was then first observed with a field emission gun – scanning electron microscope (FEG-SEM) and submitted to grazing angle X-rays. Both of these analyses were carried out without any preparation of the samples. Then thin foils for TEM were prepared that allowed imaging and analysis of the scale. SEM imaging was performed using a JEOL 6700 F microscope and TEM using a JEOL JEM 2010 microscope at University Paul Sabatier Temscan Service. The TEM apparatus used in this study operated at 200 kV and was equipped with an energy dispersive spectrometer (EDS) for chemical analysis. The values of the theoretical standard deviation for the analyzed elements (oxygen, titanium, aluminium and niobium) were very low for the conditions used and not representative of experimental scattering. An estimate of the confidence interval was thus obtained by repeating measurements in homogeneous areas of the oxide scale, giving the following values: 2 at.% for Ti, 2 at.% for Al, 5 at.% for O and 1 at.% for Nb.

For TEM and electron energy loss spectroscopy (EELS) analyses, cross sections of the oxide layer were prepared by cutting the samples into thin slices (normal to the oxide/substrate interface) with a diamond wire saw. Two slices were glued together, oxide to oxide, and embedded in a 3 mm diameter brass tube with epoxy resin. After curing, the tube was sectioned into approximately 300 μm thick discs that were then polished on their two faces and dimpled before ion-milling to transparency with a low angle (0–10°) precision ion-beam polishing system (PIPS®).

XRD data were collected in glancing incidence configuration on a Seifert XRD 3000TT apparatus fitted with a diffracted beam graphite monochromator with a 2θ step of 0.04° every 16 s. The K_α radiation of copper was used in the present study.

Furthermore, EELS analyses were recorded on an FEI TECNAI microscope at the national centre for high resolution electron microscopy (HREM) at Delft University of Technology, The Netherlands. The microscope was operated at 200 keV with a Wien filter monochromator, an improved high-tension tank, a high resolution Gatan imaging filter (HR-GIF) and a high-angle annular dark field (HAADF) detector for scanning transmission electron imaging (STEM). The present measurements were done at a total energy resolution of 0.50 eV as determined by measuring the full width at half maximum of the zero-loss peak. The following conditions were chosen to acquire the EELS spectra: an illumination semi-angle α of 1.9 mrd, a collection semi-angle β of 3.25 mrd and an energy dispersion of 0.1 eV/channel. The energy positions of the Ti–$L_{2,3}$, N–K, Al–$L_{2,3}$ and O-K edges were determined accurately using the coarse internal calibration system based on the electrostatic drift tube of the EELS spectrometer.

Reference spectra of TiO_2 rutile and anatase, alpha and gamma Al_2O_3 as well as of TiN were recorded in the same conditions as those used for analyzing the samples, in particular a probe of 1 nm in diameter. Fig. 1-a shows the Ti $L_{2,3}$ spectra of TiO_2 rutile, TiO_2

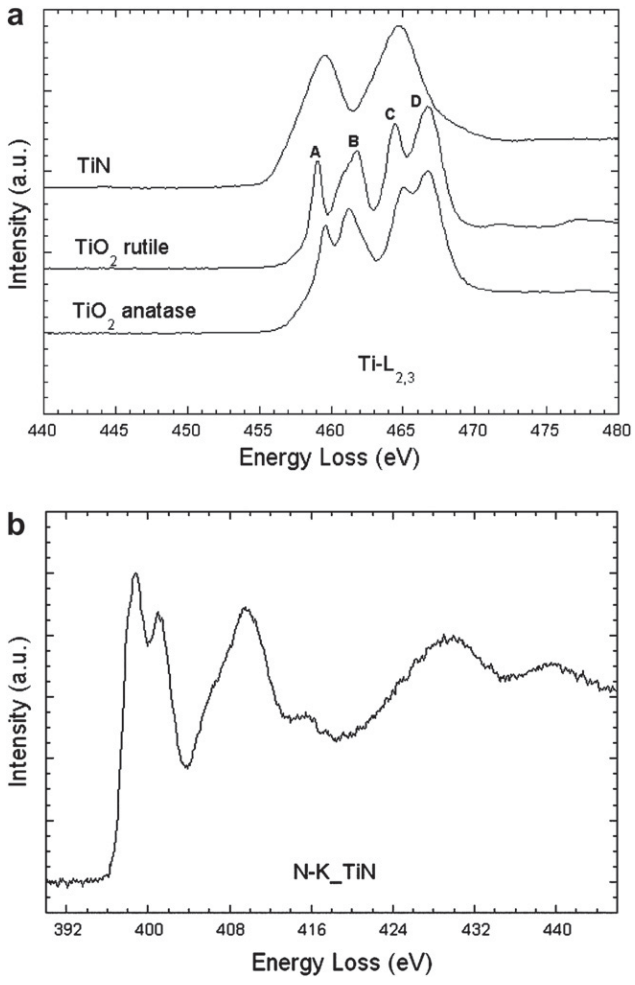

Fig. 1. (a) Ti–$L_{2,3}$ edge spectra of the reference TiN, TiO_2 rutile and TiO_2 anatase, (b) N–K edge spectra of the reference TiN.

anatase and TiN. Since intra-atomic correlations are pre-eminent, EELS Ti $L_{2,3}$ edges correspond to excitations from the $2p^6 3d^n$ Ti ground state towards the $2p^5 3d^{n+1}$ Ti states. The two major features of these edges are the strong white lines L_3 and L_2 due to the spin orbit splitting of the 2p core hole. In the case of TiO_2, the white lines are further split by the low symmetric ligand field [18]. Determining which phase of TiO_2, rutile or anatase, is present is possible due to the fact that peaks A and C of rutile are shifted to lower energy compared to anatase whereas peak B is shifted to higher energy (see Fig. 1-a). Moreover, the shape of the spectrum also plays an important role since peak B is asymmetric and this asymmetry is not the same for both phases. Note that this asymmetry can even be resolved into two peaks by high resolution X-ray absorption (XAS) [18]. Furthermore, in Fig. 1-a, the fine structure of Ti–$L_{2,3}$ edges in TiN is very different from the titanium oxides and is defined by two broad peaks corresponding to the white lines L_3 and L_2 whereas the N–K edge in TiN represented in Fig. 1-b has a specific fine structure, which strongly depends on the TiN_x structure [19]. Thus, following the changes in the Ti–$L_{2,3}$ edges indicates the presence and location of TiN or TiO_2 in the sample.

3. Results

Fig. 2 shows an FEG-SEM image of the surface of the samples oxidised for 50 and 1000 h. Most of the surface of the sample oxidised 50 h is covered with a diffuse film whilst locally bands of very fine grains can be distinguished. Close examination of the surface indicated that the diffuse film is continuous over the whole sample surface, and apparently located above the bands of grains. The surface of the sample after 1000 h of oxidation was totally covered with small grains, significantly larger than after 50 h.

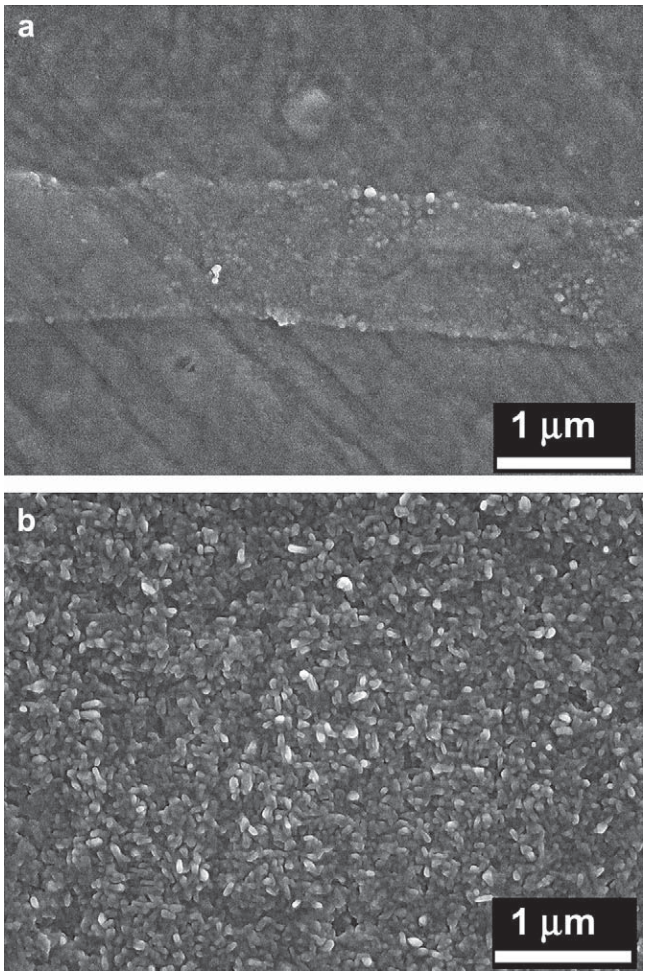

Fig. 2. Field Emission SEM image of the surface of samples heated to 700 °C in air after 50 (a) and 1000 (b) hours of exposure time.

Glancing angle X-rays were carried out on the oxidised samples and compared to the X-ray diffraction records obtained on the as-received (AR) alloy. In the case of the AR sample and of the sample oxidised for 50 h, X-ray analysis was performed only at one incidence angle $\omega = 4°$, while for the sample oxidised for 1000 h, scans for angles in the range 1–8° were recorded every single degree. Fig. 3 presents the records obtained on the AR alloy and the 50 h sample, as well as records made on the sample oxidised 1000 h for 2, 4 and 8°. It can be seen that all records show essentially the peaks related to the α_2-Ti_3Al and γ-TiAl phases of the substrate. However, comparing the records on the AR and 50 h samples, five additional faint peaks appear for the heated sample: those at 2θ equal to 42.6° and 62.7° could be associated with TiN and those at 2θ equal to 27.8, 54.3 and 62° to rutile TiO_2. It was verified that the peaks attributed to rutile could not be indexed with any of the different alumina forms (eta, gamma, theta or alpha). Independently of the value of the glancing angle, three other peaks at 2θ values equal to 34.8, 36.9 and 40.1° could be observed on the sample oxidised for 1000 h that were indexed as gamma alumina (Al_2O_3). An attempt to use the series of records at various glancing angles failed to locate the phases (Al_2O_3, TiO_2 and TiN) within the thickness of the scale.

Fig. 4 shows TEM images of the cross-section of the surface of the oxidised samples after oxidation for 50 (a) and 1000 (b) h. It is seen that both scales are bi-layered and that the thickness of the scale increased from about 250 nm to 600 nm. Many crystallites in dark contrast appear in the section of the sample oxidised for 50 h, but only in the inner layer. In contrast, the whole thickness of the scale showed fine crystallites in the 1000 h sample. It was also seen that the size of the crystallites increased from 10 to 50 nm after 50 h to up to 300 nm after 1000 h of oxidation, in agreement with the observations related to Fig. 2. In both samples, the subscale, i.e. the part of the substrate in contact with the scale, shows features differing from those of the bulk substrate but that appeared quite blurred on images such as those in Fig. 4. The thickness of the subscale also increased with oxidation time, but no well defined grains were identified in this area even after 1000 h.

Diffraction patterns were recorded such as to differentiate the outer and inner layers of the scales. A full account of these observations on the sample oxidised for 50 h was given previously [17]. It was found that the crystallites in dark contrast in the inner layer may be indexed as rutile TiO_2 while the matrix in both layers was amorphous. Furthermore, as EDS analysis showed that the outer layer was significantly poorer in Ti than the inner layer, it was suggested that the matrix consists of amorphous aluminium-rich oxide. TEM observations were repeated for the sample oxidised 50 h in other locations and it was found in many cases that the scale was solely made up of the amorphous layer. This suggests that Fig. 4-a was taken from a band of grains such as the one seen in Fig. 2, while the rest of the surface is covered only by this amorphous layer i.e. the diffuse layer mentioned earlier.

The two layers of oxide on the sample oxidised for 1000 h were similarly characterized by electron diffraction, and this showed that the amorphous matrix had crystallised. Fig. 5 presents a high magnification image of the outer layer obtained after tilting the sample so that the crystallites were well defined. Electron diffraction of the zone shown by the dotted circle in the micrograph was obtained using the selected area diaphragm under parallel illumination. This pattern was identified according to the [121] zone axis

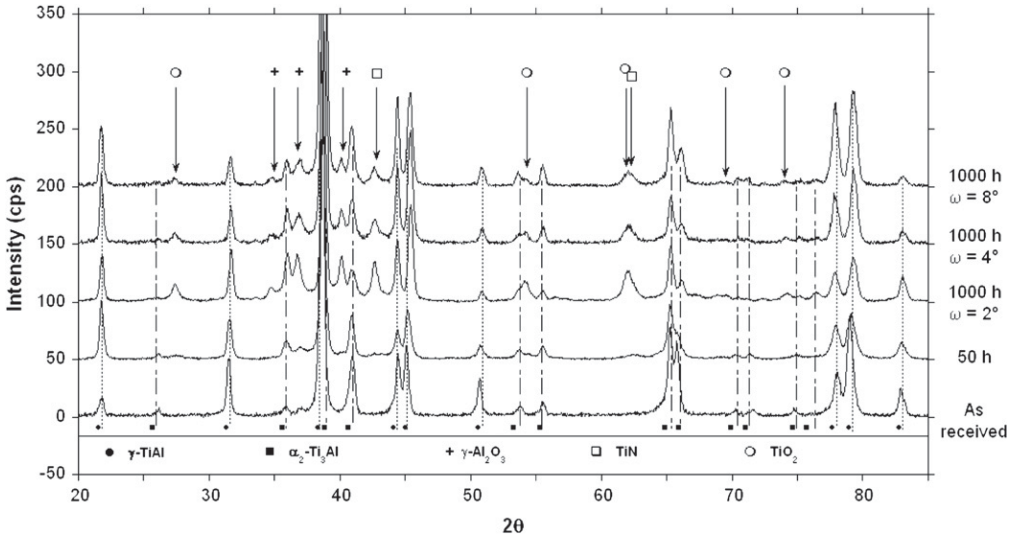

Fig. 3. Glancing angle X-rays spectra of the 50 h and 1000 h oxidised samples compared with that of the as-received (AR) material.

of cubic γ alumina with lattice parameter $a = 0.79$ nm. The corresponding reflecting planes have been indexed on the enlarged diffraction pattern in Fig. 5. Many other diffraction patterns were recorded for other crystallites in the outer layer of the scale and they were all indexed according to γ alumina.

Fig. 6 gives an example of a high magnification image from the inner layer of the sample oxidised for 1000 h, with the diffraction pattern obtained from the circled area shown on the upper right of the micrograph. As in the case of the 50 h exposure [17], the spots are arranged along circles indicating different orientations of the crystallites. These circles were indexed following the tetragonal rutile structure (with parameters $a = 0.459$ nm and $c = 0.296$ nm) and some are shown in the enlarged diffractogram in Fig. 6. In the present case, it is also possible to identify diffraction patterns from individual crystallites as shown in Fig. 6 where the spots corresponding to one TiO_2 grain oriented along [010] zone axis have been indexed. This was not possible for diffractograms obtained after 50 h oxidation, oxide crystallites being bigger and much better defined after 1000 h than after 50 h oxidation. Diffraction patterns recorded in various locations in this layer were all indexed according to the tetragonal rutile system.

While only a few discrete EDS analyses were performed on the sample oxidised for 50 h [17], composition profiles were recorded on the sample oxidised for 1000 h. Fig. 7 shows a cross section and two profiles recorded from the outer surface to depth in the subscale region. The composition values of the elements detected (titanium, aluminium, niobium and oxygen) are plotted on the graph with different symbols. One of the profiles is drawn with solid symbols and lines, while the other is shown only with empty symbols. Both profiles present very similar features, and it can be seen that the outer oxide layer (0 to about 200 nm from the outer

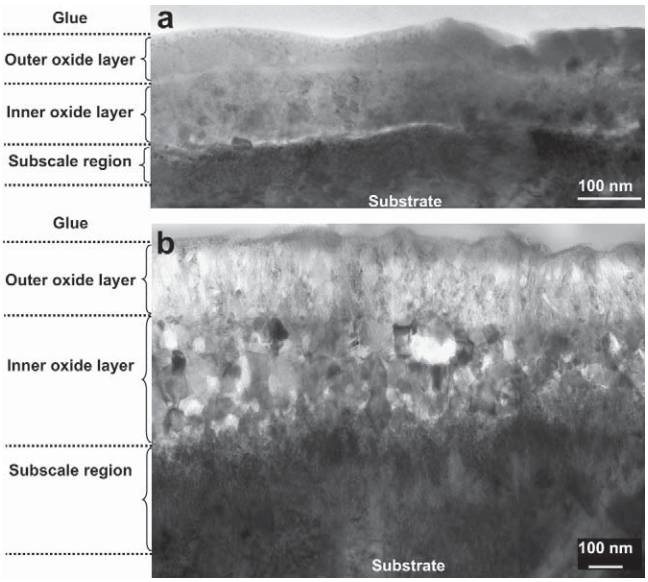

Fig. 4. Cross section TEM bright field image of the oxide scale after 50 h (a) and 1000 h (b) of oxidation.

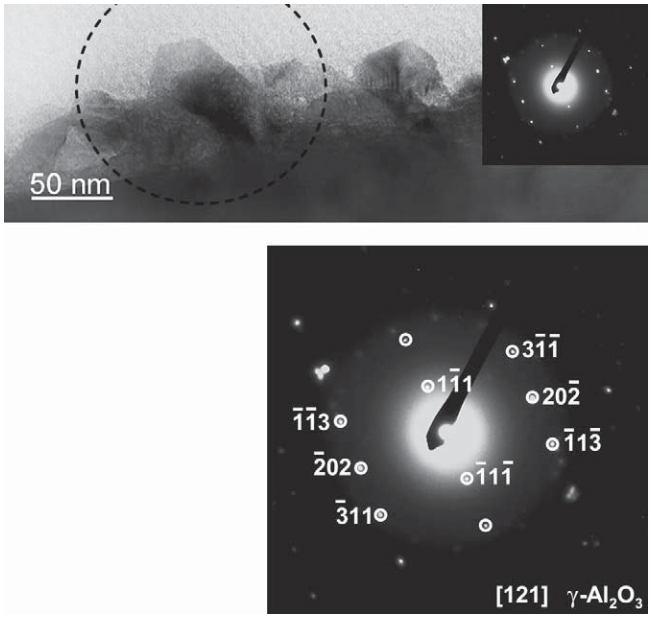

Fig. 5. High magnification cross-sectional view of the outer oxide layer after 1000 h of oxidation and diffraction pattern obtained from the well defined crystal circled in the micrograph. Indexation corresponding to the [121] zone axis of γ-Al_2O_3 is shown on the enlarged pattern.

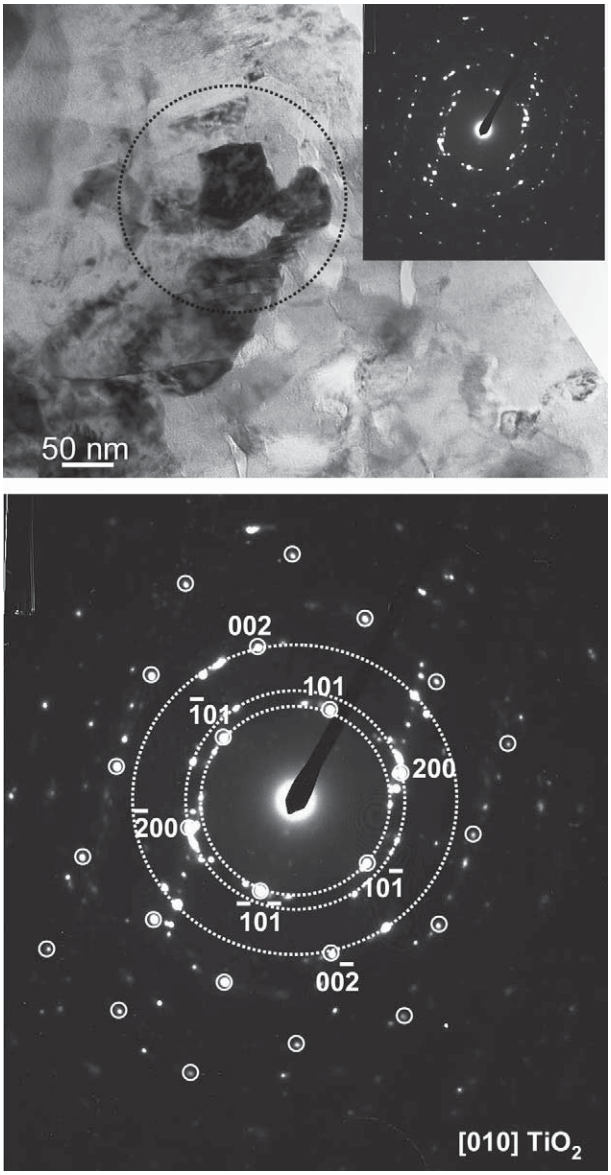

Fig. 6. High magnification image of the inner layer of the scale and diffraction pattern obtained from the circled area. Indexation according to rutile – TiO_2 is shown on the enlarged pattern.

surface) mainly contains aluminium and oxygen, with low amounts of titanium and no traces of niobium. Taken together with the diffraction pattern shown in Fig. 5, these results lead to the conclusion that the outer layer of the scale consists only of gamma alumina. At the transition between the outer and inner layers, the amount of titanium increases rapidly and stabilises at about 39–45 at.%, while the level of aluminium decreases to about 5–6 at.%. This layer contains some Nb, up to about 5–7 at.%, and an oxygen content similar to that of the outer layer (48 at.%). Together with the diffraction results (Fig. 6), these data show that the inner layer consists entirely of rutile TiO_2. At the transition between the outer and inner layers, the scale is made of intermixed alumina and titania grains through a thickness of about 50 nm.

The transition between the scale and the subscale is characterized by a sharp decrease in the oxygen content and an increase in the aluminium content taking place over about 200 nm (600–800 nm in Fig. 7). In this transition region, a clear increase of the titanium content is also observed, as well as a slight increase of the

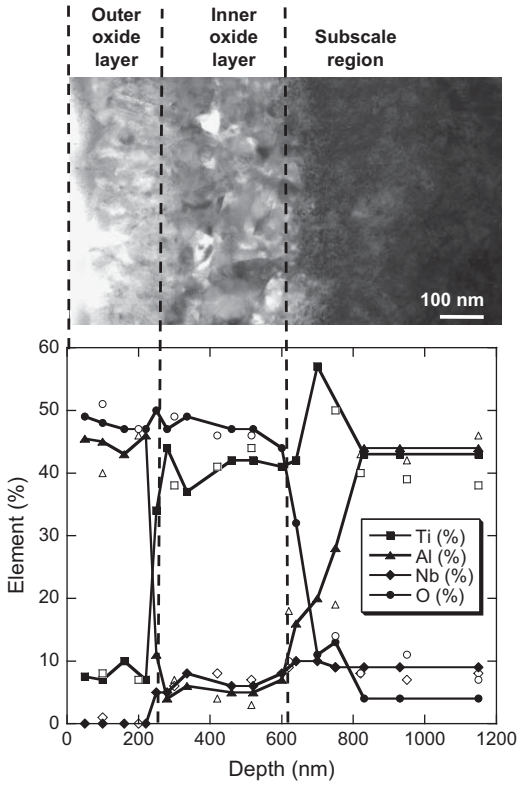

Fig. 7. Cross section view and composition profiles for the elements listed in the graph after two series of EDS spot analyses of the scale and subscale.

niobium content. After this transition region, further towards the substrate, the composition of the subscale is nearly constant though a few Nb-rich particles were observed as was also the case for the sample oxidised for 50 h [17]. As nitrogen cannot be analyzed by EDS, EELS was then used to locate the TiN precipitates highlighted in the X-ray diffractograms of the sample oxidised for 50 h. This technique was then applied to characterize the interface between the inner oxide layer and the subscale region of the sample oxidised for 1000 h.

In order to better visualize the scale of the samples, HAADF imaging in the STEM mode in the TECNAI microscope was used as it offers the advantage of an incoherent signal (to avoid unwanted Fresnel effects) and an increased atomic number contrast. A combination of STEM and EELS techniques thus enables us to probe the Ti–L edges on the nanometer scale in order to identify the chemical nature of the different layers. Fig. 8-a shows an STEM HAADF image of the scale of the sample oxidised for 50 h. Several EELS spectra of Ti–$L_{2,3}$, N–K and O–K edges were recorded in the middle of the oxide layer that showed the presence of some small crystals of rutile TiO_2 and of alumina. The different peaks related to this latter phase have the same shape as those of γ-Al_2O_3 [20] but are broader, possibly due to the amorphous state of the matrix. These results are thus in line with the TEM observations showing crystallised rutile grains within an Al-rich amorphous matrix.

In some locations at the interface between the oxide layer and the subscale region, the position and shape of Ti–$L_{2,3}$ edges were found to be equivalent to the reference TiN as illustrated by the spectrum in Fig. 8-b that corresponds any of the two dots in Fig. 8-a. Though the N–K edge is very noisy due to the small amount of this phase, it clearly matches that of reference TiN. The presence of the same kind of alumina as above was also noticed, indicating the simultaneous presence of small inclusions of TiN and Al_2O_3 in the oxide layer at the interface with the subscale region.

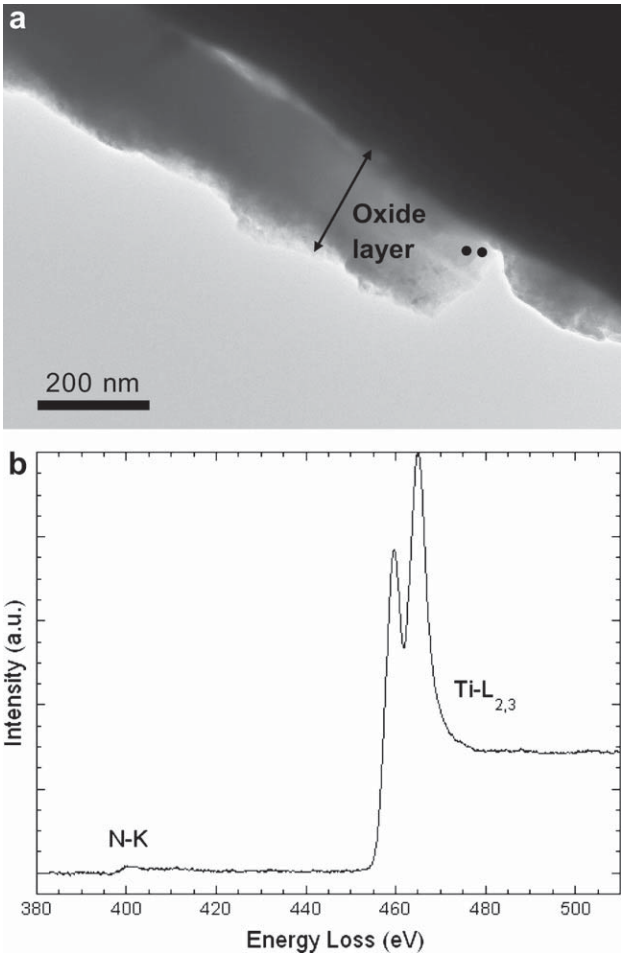

Fig. 8. a) STEM HAADF image of the sample oxidised for 50 h; b) Ti–$L_{2,3}$ and N–K edge spectrum in the oxide layer at the interface with the subscale region (locations shown with dots in a).

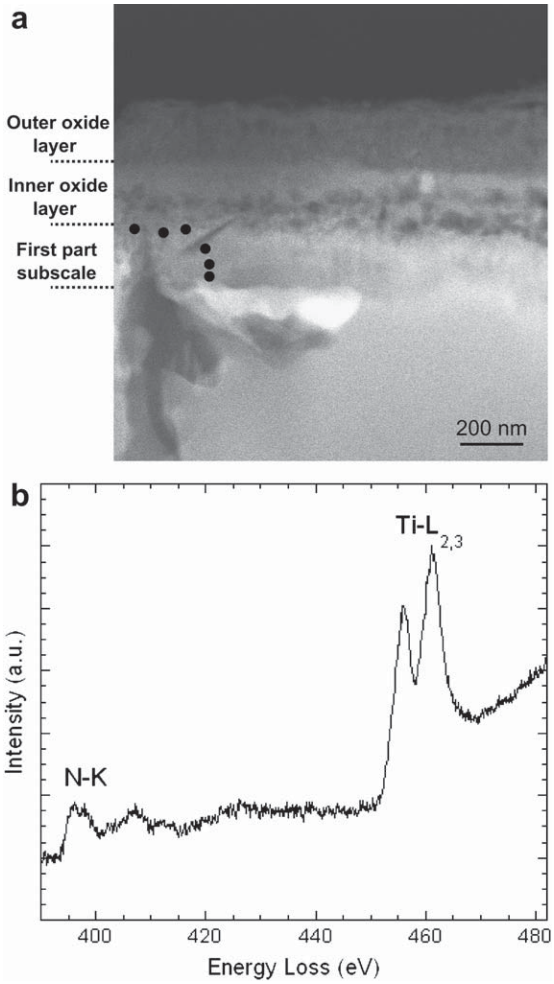

Fig. 9. a) STEM HAADF image of the sample oxidised for 1000 h; b) example of the Ti–$L_{2,3}$ and N–K edge spectrum as recorded on the first part of the subscale region (solid dots in a).

Different spectra (with both Ti–$L_{2,3}$ and N–K edges) were recorded in the inner oxide layer and in the first part of the subscale region of the sample oxidised 1000 h. The locations of the probe are shown with dots on the STEM HAADF in Fig. 9-a. In the inner oxide layer, the signature of nitrogen (N–K edge) was not detectable, whilst the position and shape of Ti–L edges were found to be equivalent to the reference TiO_2 rutile. In agreement with the above conclusion of the TEM study, this layer is predominantly made of TiO_2 rutile. Several core-line spectra (with both Ti–$L_{2,3}$ and N–K edges) were recorded across the outer (or first) part of the subscale as well as single EELS spot (probe size: 1 nm). All scans were composed of 50 spectra corresponding to a maximum acquisition time of 2 min in order to minimize contamination as well as irradiation and instability effects. The evolution of the N–K edges and Ti–$L_{2,3}$ fine structures from one spectrum to another was always the same and is illustrated by the spectra shown in Fig. 9-b. The characteristics of these spectra are those of the reference sample TiN. Thus, the layer enriched in Ti that appeared at the outer part of the subscale in Fig. 7 is composed of TiN.

4. Discussion

Working with the same alloy as that investigated here, Godlewska et al. [21,22] and Teng et al. [14] also observed, as expected from the introduction, the formation of alumina rich scale following short term oxidation. After oxidation under air for 40 h at 800 °C, Godlewska et al. [21] found that 90% of the scale was still composed of alumina. However, at temperatures in the range 900–1200 °C, Teng et al. [14] observed that a TiO_2 outer layer forms after sufficient oxidation, and this was recently confirmed by Ebach–Stahl et al. at 900 and 1000 °C [23]. This is in agreement with the results of oxidation under air at 900 °C performed by Lang and Schütze [4] and Zhao et al. [13] who compared the behaviour of ternary Ti–Al–Nb alloys to their binary counterparts. After 4 h of exposure, a TiO_2 outer layer is not present on the scale of a Ti–35Al–5Nb alloy while it is on its binary counterpart [4]; the same is true after oxidation for 90 min of a Ti–45Al–8Nb alloy [13]. At 704 °C, the scale formed after oxidation of a Ti–48Al–2Cr–2Nb alloy is a mixture of alumina and rutile after 1000 h, while an outer rutile layer has formed after 6000 h [8]. This suggests that by lowering the oxidation kinetics, the addition of Nb also delays the formation of the outer TiO_2 scale but that this latter will appear anyway after sufficient oxidation time. The time it starts to appear seems to be delayed on increasing the Nb content, so it would be expected to occur after a very long time (several thousand hours) at 700 °C for the present alloy as compared to the alloy studied by Locci et al. [8].

As reviewed previously [17] the transient formation of amorphous alumina during oxidation at intermediate and high temperatures has already been reported for TiAl and other alloys.

For the present alloy, it may be more precise to call this an aluminium-rich amorphous oxide as EDS measurements showed it to contain 14 at.% Ti, though without Nb. The present observations suggest that, during the oxidation process, the whole surface gets covered with a film of such an amorphous phase. In a second step, TiO_2 crystallises within the amorphous scale leading to a two-layered structure which is already well established after 50 h. The detection of both TiN and alumina at the interface between the scale and the substrate suggests that the oxidation mechanism is the same at 700 °C as at higher temperatures. Accordingly, TiO_2 would form by oxidation of TiN precipitates, the rejected nitrogen further supporting the process: the TiN layer is seen to grow with oxidation time, as already observed at the same temperature [8]. EDS measurements showed that when alumina crystallises it rejects Ti, and this must lead to an increased amount of TiO_2 in the scale. Interestingly enough, it is seen that this does not imply early formation of rutile on the outer part of the scale at the temperature investigated.

5. Conclusion

Isothermal oxidation of a TiAl–8Nb alloy at 700 °C gives rise to a two-layered scale consisting in an outer Al-rich amorphous oxide layer and an inner oxide layer made of fine rutile crystallites in an Al-rich amorphous oxide matrix. After a short oxidation period (50 h), no distinct nitride precipitates were observed in TEM, although some indications of TiN were obtained from glancing XRD and were further confirmed with EELS.

After long-term oxidation (1000 h), the scale was found to have a similar bi-layered structure. In this latter case however, the scale was thicker than for the short oxidation period and the outer alumina layer crystallised completely to give fine γ-alumina grains. At that stage, the inner oxide layer was made of fine rutile crystallites and the transition zone between the two layers was actually a thin intermixed region of both rutile and gamma alumina.

It was also observed that the first part of the subscale, directly in contact with the scale, contains titanium nitrides that form a continuous layer after 1000 h of oxidation. The inner part of the subscale that is directly in contact with the substrate appeared to be slightly Al depleted, though no traces of α_2-Ti_3Al were detected, suggesting that at the temperature studied here and for up to 1000 h exposure, Al depletion is not sufficiently pronounced to form such a phase. Work is in progress to fully characterize the inner part of the subscale in relation with bulk microstructure.

Acknowledgements

The present work was carried out within the framework of the European project IMPRESS (Intermetallic Materials Processing in Relation to Earth and Space Solidification), contract FP6-500635. The authors thank Alistore European Network of excellence for the microscopy platform facilities at TU Delft.

References

[1] Meier GH, Pettit FS. Microstructural Science 1996;24:155–65.
[2] Taniguchi S, Shibata T. Intermetallics 1996;4:S85–93.
[3] Choudhury NS, Graham HC, Hinze JW. In: Foroulis ZA, Pettit FS, editors. Properties of high temperature alloys. The Electrochemical Society; 1976. p. 668–80.
[4] Lang C, Schütze M. Materials and Corrosion 1997;48:13–22.
[5] Meier GH, Appalonia D, Perkins RA, Chiang KT. In: Grobstein T, Doychak J, editors. Oxidation of high-temperature intermetallics. TMS; 1988. p. 185–93.
[6] Brady MP, Pint BA, Tortorelli PF, Wright IG, Hanrahan RJ. In: Schütze M, editor. Materials science and technology, corrosion and environmental degradation. VCH; 2000. p. 229–325.
[7] Rakowski JM, Pettit FS, Meier GH, Dettenwanger F, Schumann E, Ruhle M. Scripta Metallurgica et Materialia 1995;33:997–1003.
[8] Locci IE, Brady MP, MacKay RA, Smith JW. Scripta Materialia 1997;37:761–6.
[9] Dettenwanger F, Schumann E, Rakowski J, Meier GH, Rühle M. Materials and Corrosion 1997;48:23–7.
[10] Dettenwanger F, Schumann E, Rühle M, Rakowski J, Meier GH. Oxidation of Metals 1998;50:269–96.
[11] Guo C, Zhang C, Lu W, He L, Xi Y, Wang F. Oxidation of Metals 2007;68:65–76.
[12] Lu W, Chen C, He LL, Wang FH, Lin JP, Chen GL. Corrosion Science 2008;50:978–88.
[13] Zhao LL, Lin JP, Chen GL, Wang YL. In: Kim Y-W, Morris D, editors. Structural aluminides for elevated temperatures. Warrendale: TMS; 2008. p. 275–88.
[14] Teng L, Nakatomi D, Seetharaman S. Metall Mater Trans B 2007;38:477–84.
[15] Jiang H, Hirohasi M, Lu Y, Imanari H. Scripta Mater 2002;46:639–43.
[16] Lu W, Chen C, Xi Y, Guo C, Wang F, He L. Intermetallics 2007;15:989–98.
[17] P.E. Tchoupé Ngnekou, M.-C. Lafont, F. Senocq, J. Lacaze, B. Viguier, Proceedings of the conference Materiais; 2009, CD-ROM edited by Instituto Superior Técnico, Lisboa. To appear in Materials Science Forum.
[18] Ruus R, Kikas A, Saar A, Ausmees A, Mommiste E, Aarik J, et al. Solid State Communications 1997;104(4):199–203.
[19] C. Mirguet, PhD thesis, CEMES Toulouse; 2004.
[20] Bouchet D, Colliex C. Ultramicroscopy 2003;96:139–52.
[21] Godlewska E, Mitoraj M, Devred F, Nieuwenhuys BE. Journal of Thermal Analysis and Calorimetry 2007;88:225–30.
[22] Godlewska E, Mitoraj M, Morgiel J. Materials at High Temperatures 2009;26: 99–103.
[23] Ebach-Stahl A, Frölich M, Leyens C. Materials at High Temperatures 2009;26: 91–7.